JOURNAL OF AIRCRAFT
Vol. 43, No. 1, January–February 2006

Effects of Winglet Dihedral on a Tip Vortex

P. Gerontakos* and T. Lee†
McGill University, Montreal, Quebec H3A 2K6, Canada

The effect of winglet dihedral ($-87.5 \leq \delta \leq 87.5$ deg) on the near-field tip vortex flow structure behind a swept and tapered NACA 0015 wing was investigated at $Re = 1.81 \times 10^5$. The winglet dihedral led to a significantly reduced (increased) peak tangential velocity and vorticity (core radius) compared to a baseline wing. The values of core circulation (core axial velocity) could be below or above the baseline-wing value, depending on the winglet angle, and exhibited a local maximum (minimum) at $\delta = 0$ deg. The inner region of the tip vortex flow exhibited a self-similar behavior for a wing with and with no winglet. The lift-induced drag was always reduced by the addition of a winglet. The negative dihedral was more effective in reducing the lift-induced drag compared to the corresponding winglet of positive dihedral. A large discrepancy in the lift-induced drag was, however, observed between the wake integral method and the classical lifting-line theory.

Nomenclature

AR	=	aspect ratio, b^2/S
b	=	(semi-)wing span
C_D	=	total drag coefficient
C_{Di}	=	lift-induced drag coefficient, $D_i/\frac{1}{2}\rho {u_\infty}^2 S$
C_L	=	lift coefficient
c	=	chord
D_i	=	lift-induced drag
L	=	lift force
Re	=	Reynolds number, $u_\infty c_r/\nu$
r	=	radial position
r_c	=	core radius
r_o	=	outer radius
S	=	wing area
u	=	axial mean velocity
u_c	=	core axial velocity
u_∞	=	freestream velocity
v	=	transverse mean velocity
v_θ	=	tangential velocity
w	=	spanwise mean velocity
x	=	streamwise or axial direction
y	=	transverse direction
z	=	spanwise direction
α	=	angle of attack
Γ	=	circulation or vortex strength
Γ_b	=	bound circulation
Γ_c	=	core circulation
Γ_o	=	total circulation
δ	=	winglet dihedral
ζ	=	streamwise vorticity
Λ	=	sweep angle
λ	=	taper ratio, c_t/c_r
ν	=	kinematic viscosity
ρ	=	fluid density
σ	=	source term in Eq. (3), $\partial v/\partial y + \partial w/\partial z$
ϕ	=	velocity potential
ψ	=	stream function

Received 19 October 2004; revision received 27 January 2005; accepted for publication 27 January 2005. Copyright © 2005 by P. Gerontakos and T. Lee. Published by the American Institute of Aeronautics and Astronautics, Inc., with permission. Copies of this paper may be made for personal or internal use, on condition that the copier pay the $10.00 per-copy fee to the Copyright Clearance Center, Inc., 222 Rosewood Drive, Danvers, MA 01923; include the code 0021-8669/06 $10.00 in correspondence with the CCC.

*Graduate Research Assistant, Department of Mechanical Engineering, 817 Sherbrooke Street West.

†Associate Professor, Department of Mechanical Engineering, 817 Sherbrooke Street West. Member AIAA.

Introduction

THE counter-rotating longitudinal vortices generated by aircraft wing tips, because of their hazardous effects on flight safety, continue to be of concern to the aviation industry and aircraft manufacturers alike. Moreover, tip vortices shed from helicopter rotor blades and propellers interact with following blades causing excessive rotor noise and vibration. Therefore, to reduce the flight time and separation distance of aircraft during takeoff and landing, as well as to reduce the tip vortex-induced drag and noise, the trailing vortex wake characteristics must be measured and predicted accurately and reduced or eliminated, if possible.

Various passive[1–7] and active[1,8,9] tip geometry modification devices, such as endplates, winglets and tip sails, tailored and raked wingtips, and steady or pulsating blowing jets of air into the vortex region, have been proposed to minimize the strength of the trailing vortex and to reduce the lift-induced drag. Among them, the winglet has been widely recognized as a more efficient means of improving cruise drag performance than a simple spanwise tip extension with the same structural weight penalty. The wing-tip-mounted, nearly vertical winglet can also develop a normal force that alters the configuration span load to diffuse the total circulation in the rolled-up wing-tip vortex and reduce the total energy of the vortex. The basic physical effect of the winglets,[2] which leads to drag reduction, is a vertical diffusion of the tip vortex flow, at least just downstream of the tip, which substantially reduces the magnitudes of the crossflow behind the tip. Also, the presence of a lower winglet lessens the induced velocities on the upper winglet and results in a decreased boundary-layer separation on the winglet inner surface.

Recently, Eppler[6] suggested that a spanwise tip extension with a dihedral of about 10 deg rendered a lower induced drag than a planar wing with the same length through the nonlinear effect of induced lift, which had the effect of decreasing the induced drag for a given lift. The induced lift was caused by the velocity that lifting vortices induced on themselves and did not develop on a planar wing. Furthermore, although the span was reduced by deflecting the tip, the wing performed better than a planar wing with the same length, or wetted area. Gold and Visser[7] later examined the impact of the dihedral on the performance of a swept and tapered NACA 0012 wing fitted with a winglet and reported that the negative dihedral yielded a lower lift-induced drag than the zero and positive dihedral configurations.

In summary, despite much work, the bulk of the experimental investigations were mainly concentrated on direct wind-tunnel force balance and surface pressure measurements. Detailed surveys of the tip-vortex flow structure behind a winglet, especially in the near wake of the generating wing, are still needed. The objective of the present study was to investigate the three-dimensional flow structure of the tip vortex in the near field behind a sweptback and tapered NACA 0015 wing with and without a winglet of different

dihedrals by using a miniature seven-hole pressure probe at a root-chord Reynolds number $Re = 1.81 \times 10^5$. Particular attention was focused on the effects of the winglet dihedral on the variation of the crossflow and axial velocity and vorticity distributions and the strength, size, and trajectory of the vortex, as well as the estimation of the bound and spanwise circulation. Lift-induced drag was computed using a wake integral method and was compared with the wind-tunnel force balance data.

Experimental Apparatus and Methods

The experiment was carried out in the new $0.9 \times 1.2 \times 2.7$ m suction-type wind tunnel at McGill University with a freestream turbulence intensity of 0.03% at 35 m/s. An untwisted sweptback and tapered wing, made of solid aluminum, with an aspect ratio AR of 3.654, a taper ratio λ of 0.375, a semispan b of 51 cm, and a wing area S of 713 cm^2 was used as the baseline test model. The root chord c_r was 20.3 cm, and the tip chord c_t was 7.6 cm. The sweep angle Λ at one-quarter-chord location was set at 24 deg. The square-tipped baseline wing had a NACA 0015 section throughout. The wing model was mounted horizontally at the center of the sidewall of the wind-tunnel test section (Fig. 1). A circular endplate of 50 cm diameter with a sharp leading edge was fitted to the one end, adjacent to the tunnel sidewall, of the wing model to isolate the free end effects. The origin of the coordinate system was located at the trailing edge of the root of the wing with the x, y, and z axes in the streamwise, transverse, and spanwise directions, respectively. An untwisted winglet of a NACA 0015 section with $b = 6.24$ cm, $\lambda = 0.518$, AR $= 1.08$, and $\Lambda_{c/4} = 35$ deg was added to the tip of the baseline wing. The dihedral of the winglet was set at $\delta = 0$ (a raked tip or a simple spanwise tip extension), ± 20, ± 40, ± 67.5, and ± 87.5 deg (which approximates a simple endplate). The joint between the baseline wing tip and the winglet had a body of revolution of NACA 0015 airfoil section. Detailed configurations and dimensions of the baseline wing and the winglet are also given in Fig. 1 and Tables 1 and 2. All coefficients were defined at the same total lift based on the baseline wing geometry at $\alpha = 8$ deg with $C_L = 0.73$. The freestream velocity u_∞ was fixed at 13.84 m/s, which rendered a root-chord Reynolds number of 1.81×10^5.

A miniature seven-hole pressure probe (with an outside diameter of 2.6 mm) was used to measure the three mean velocity components, u, v, and w, at three distances downstream of the wing trailing edge, $x/c_r = 0.75$, 1.5, and 2.75 or $x/c_t = 0.267$, 2.267, and 5.601. Each data plane taken in the near field of the wing models had 33×85 measuring grid points with an increment of $\Delta y = \Delta z = 3.2$ mm, except along the span of the wing, where $\Delta z = 6.4$ mm. The probe was calibrated in situ, following the calibration procedures described by Wenger and Devenport,[10] before the installation of the model. Eight pressure transducers (seven for the probe and one for tunnel reference static pressure) were used to maximize the data rate of the probe measurement system at each measurement location. The pressure signals were sampled at 500 Hz, with a sampling time of 5 s, and were recorded on a personal computer through a 16-bit A/D converter board. Probe traversing was achieved through a custom-built computer-controlled traversing system. Note that, due to the limitation of the probe traversing mechanism, the present wake survey region did not encompass the entire wing; only 85% of the wing wake (covering $0.375 \le z/c_r \le 2.76$ or $0.15 \le z/b \le 1.1$) was measured. The lift-induced drag coefficients C_{Di} ($= D_i / \frac{1}{2}\rho u_\infty{}^2 S$, where D_i is the induced drag and ρ is the fluid density) were also computed based on the vorticity distributions inferred from the measured crossflow fields and were compared with the wind-tunnel force-balance data and the classical lifting-line theory as well. No boundary-layer transition strips were placed on the upper or lower surfaces of the wing model.

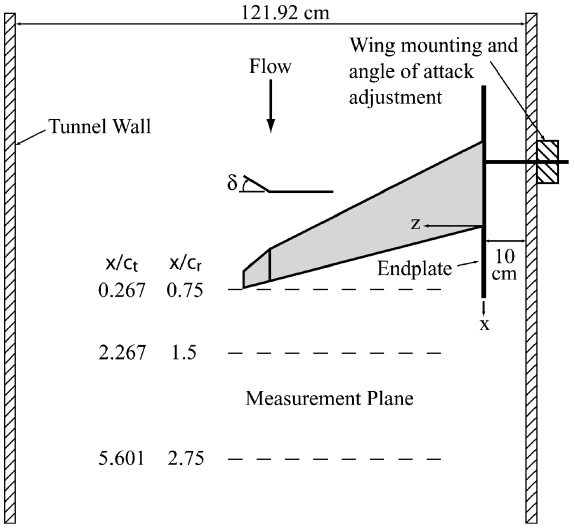

Fig. 1 Schematics of wing model and experimental setup.

Table 1 NACA 0015 airfoil properties

Wing		Winglet	
Parameter	Value	Parameter	Value
C_r	20.32 cm	C_{wr}	7.62 cm
C_t	7.62 cm	C_{wt}	3.95 cm
$b_{c/4}$	55.88 cm	$b_{c/4}$	7.62 cm
b	51.05 cm	b	6.24 cm
Λ_{LE}	26.9 deg	Λ_{LE}	40.27 deg
$\Lambda_{c/4}$	24 deg	$\Lambda_{c/4}$	35 deg
Λ_{TE}	14.5 deg	Λ_{TE}	14.52 deg
S	713.15 cm^2	S	36.10 cm^2
AR	3.654	AR	1.079
λ	0.375	λ	0.518

Table 2 Wing/winglet configuration

	δ, deg				
Parameter	0	± 20	± 40	± 67.5	± 87.5
b_{total}, cm	57.29	56.91	55.83	53.44	51.32
S_{total}, cm^2	749.25	747.07	740.80	726.96	714.72
AR_{total}	4.381	4.335	4.208	3.928	3.685

For lift and drag force measurements, the wing models were mounted vertically on an external two-component force balance located below the wind tunnel. Details of the force-balance measurement system are given by Birch et al.[11] The maximum experimental uncertainties in the results reported have been estimated as follows[11]: mean velocity 3.5%, vorticity component 8%, vortex radius 4%, and velocity fluctuation 3%. The vortex meandering in the near field behind the generating wing was examined by using the correlation technique/criteria employed by Chow et al.[12] The meandering of the vortex was determined to be small and did not contribute appreciably to the present measurements.

Results and Discussion

Baseline Wing

To facilitate the investigation of the effect of the winglet dihedral on the tip-vortex flow, the three-dimensional flow structure of the tip vortex behind a baseline, or clean, wing was characterized first and serves as a comparison. Figures 2a and 2b show the typical nondimensional vw velocity vectors and axial and vorticity contours behind a baseline wing at $x/c_r = 2.75$ for $\alpha = 8$ deg. For clarity, only $1.75 \le z/c_r \le 2.75$ wake flow measurements are shown here. The dashed lines denote the trailing edge of the wing. Two distinct flow structures can be clearly seen in the flowfield: the wing wake and the trailing tip vortex (Fig. 2a). Outside the wake and tip vortex regions, the vorticity ζ was essentially zero and the axial velocity u attained the value of the freestream u_∞. The majority of the vorticity was found to be located in the small and concentrated core of the tip vortex (Fig. 2b, where numerical values denote u/u_∞ and $\zeta c_r/u_\infty$ levels with increments of 0.02 and 4.0, respectively). At $x/c_r = 2.75$, the inner region of the tip vortex was well developed

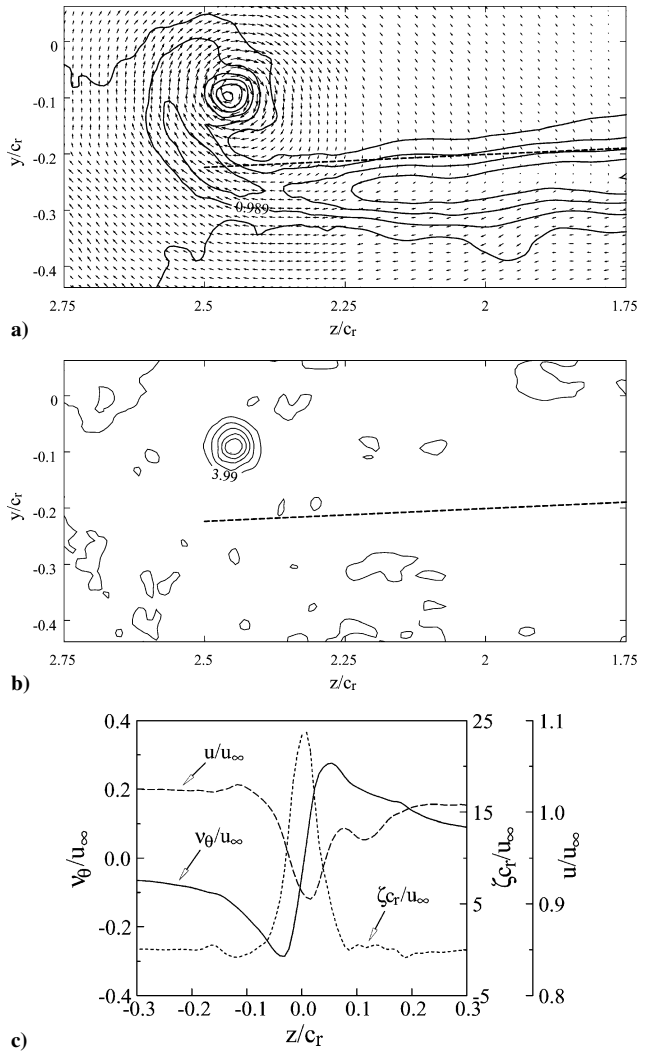

Fig. 2 Nondimensional a) crossflow velocity vectors overlaid with mean axial velocity contours, b) contours of mean streamwise vorticity for a baseline wing at $x/c_r = 2.75$, $\alpha = 8$ deg, and c) composite of v_θ/u_∞, $\zeta c_r/u_\infty$, and u/u_∞ distributions through the vortex.

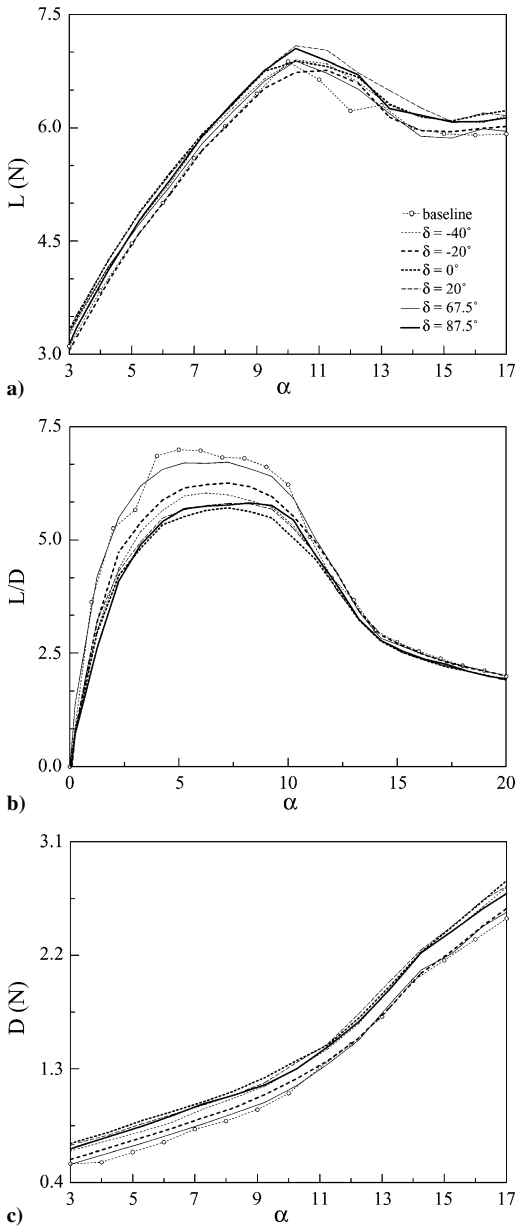

Fig. 3 Wing loads a) lift force, b) lift-to-drag ratio, and c) drag force.

and nearly axisymmetric and had a core radius r_c (defined by the location of maximum tangential velocity $v_{\theta\text{peak}}$) of $0.043c_r$ (Fig. 2c). Outside the core, the flow structure was dominated by the remainder of the wing wake, which wound into an ever-increasing spiral. The ***vw*** vectors suggest a typical vortex circulation: The tangential velocity v_θ varied nearly linearly from zero to $v_{\theta\text{peak}}$ with the radius in the inner flow region, while varying with r^{-1}, and asymptotically approached zero in the outer flow region (Fig. 2c). Figure 2c also indicates that the vorticity was highest at the center of the vortex, approached zero outside of the core, and had a bell-shaped wakelike axial velocity distribution, which is similar to the turbulent wake behind a circular cylinder. The results also indicate that, for a baseline wing, the point of maximum velocity deficit, or core axial velocity u_c, coincided with the vortex center (located by the location of ζ_{peak}), within measurement error, suggesting the near completion of the rollup of the shear layers in the inner region of the tip vortex for $x/c_r \geq 0.75$. In summary, a $v_{\theta\text{peak}} = 0.3u_\infty$, $\zeta_{\text{peak}} = 24.0u_\infty/c_r$ accompanied by an $r_c = 0.043c_r$ and $u_c = 0.905u_\infty$ was observed at $x/c_r = 2.75$. Also, for $1 \leq x/c_r \leq 2.75$, the core radius remained basically unchanged, whereas u_c was observed to vary. Furthermore, the center of the circulation appeared to be inboard from the tip and above the wing in the near field before it finally moved down.

The baseline wing results also show that both the core Γ_c and total Γ_o circulation of the tip vortex remained virtually unchanged with $\Gamma_c/u_\infty c_r = 0.074$ and $\Gamma_o/u_\infty c_r = 0.117$, which rendered a Γ_c/Γ_o of 0.63 (compared to the theoretical value of $\Gamma_c/\Gamma_o = 0.71$ for Lamb's solution[13]), in the near field at $x/c_r = 2.75$. The circulation or vortex strength was determined by employing Stokes's theorem. The present experiment also shows a total circulation-to-bound circulation $(\Gamma_o/u_\infty c_t)/(\Gamma_b/u_\infty c_r)$ ratio of 0.4, which suggests that in the near field behind a swept and tapered wing about 40% of the bound circulation was entrained into the tip vortex. The bound vorticity Γ_b was determined from classical Prandtl's lifting-line theory,

$$\Gamma_b/u_\infty c_r = \tfrac{1}{2}(K_1 C_L + K_2) \tag{1}$$

with constants K_1 and K_2 determined following the method of Glauert.[14] $C_L = 0.73$ was obtained directly with a force balance (Fig. 3). Note that the present whole wake flow measurements also allow the estimation of the bound circulation at the root from the spanwise circulation $\Gamma(z)$ distribution along the wing span (open circles in Fig. 4). $\Gamma_{b,m}/u_\infty c_r$ of about 0.290 was obtained at the root of the wing model tested. The measured bound circulation $\Gamma_{b,m}$ was found to be about 18% lower than the bound circulation $(\Gamma_b/u_\infty c_r = 0.352)$ determined from Eq. (1). Figure 4 also shows that there was a dip in the spanwise $\Gamma(z)$ distribution near the tip, implying the existence of a tip vortex with a stronger vortex circulation accompanied by a higher lift-induced drag, compared to an

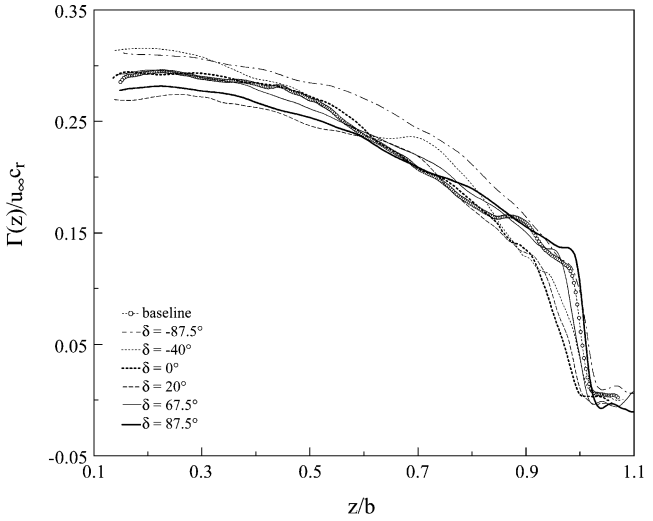

Fig. 4 Spanwise circulation distribution.

elliptically loaded wing at the same total lift force and Reynolds number. The spanwise $\Gamma(z)$ distributions also allow the calculation of lift distribution via

$$L = \rho_\infty u_\infty \int_{-b/2}^{b/2} \Gamma(z)\,\mathrm{d}z \tag{2}$$

when instrumentation limitations or small scales of the experimental setup prohibit direct measurements of the airloads from pressure distributions. The lift coefficient determined from Eq. (2) was found to be in good agreement with the force-balance measurements, indicating that the circulation distributions were consistent with the measured lift data according to the Kutta–Joukowski theorem.

Finally, the lift-induced drag coefficient C_{Di}, which is directly related to the crossflow energy, was also computed from the vorticity inferred from the measured velocity field by using the Maskell induced-drag model[15] at different downstream distances. The ***vw*** crossflow velocity vectors within the measurement plane were decomposed into a stream function $\psi\ (y, z)$ and a velocity potential $\phi\ (y, z)$ with the imposed boundary conditions requiring both ψ and ϕ

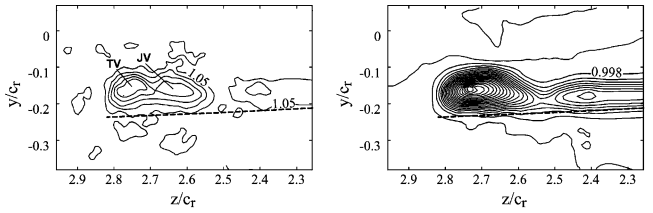

a) $\delta = 0$ deg, $x/c_r = 0.75$

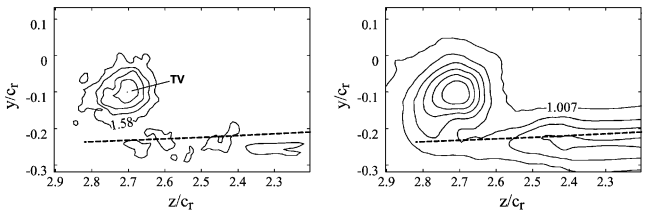

b) $\delta = 0$ deg, $x/c_r = 2.75$

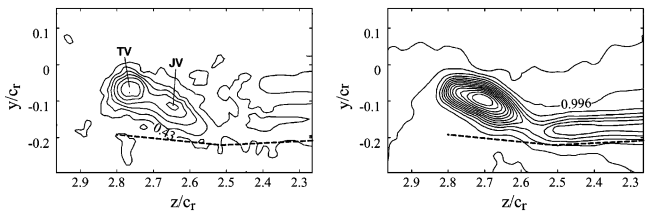

c) $\delta = 20$ deg, $x/c_r = 0.75$

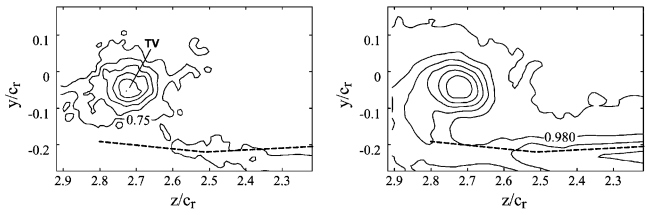

d) $\delta = 20$ deg, $x/c_r = 2.75$

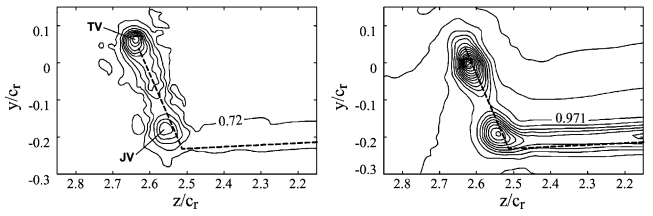

e) $\delta = 67.5$ deg, $x/c_r = 0.75$

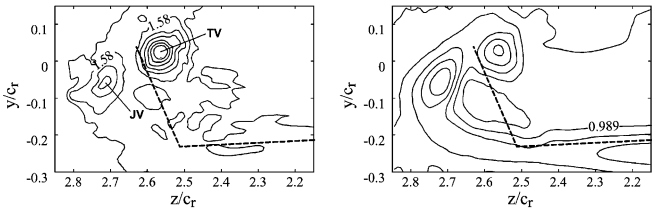

f) $\delta = 67.5$ deg, $x/c_r = 2.75$

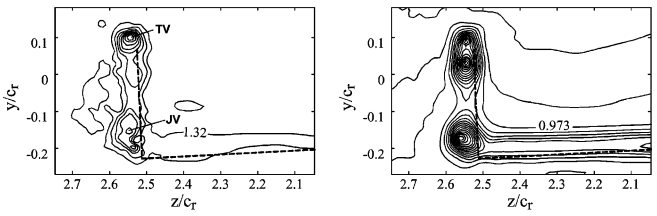

g) $\delta = 87.5$ deg, $x/c_r = 0.75$

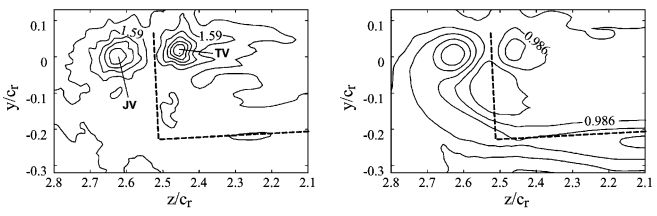

h) $\delta = 87.5$ deg, $x/c_r = 2.75$

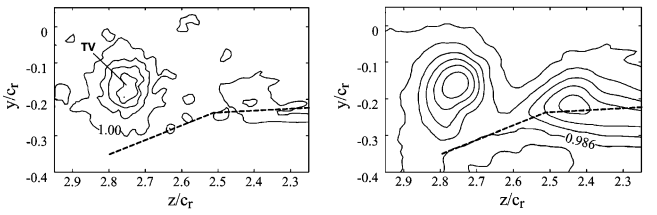

i) $\delta = -20$ deg, $x/c_r = 2.75$

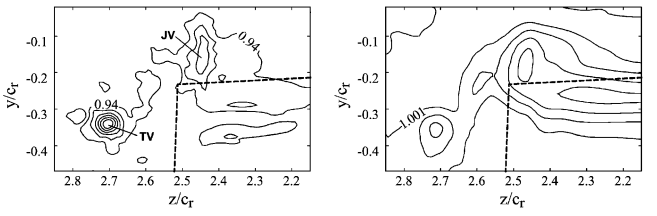

j) $\delta = -87.5$ deg, $x/c_r = 2.75$

Fig. 5 Nondimensional contours of streamwise vorticity and axial velocity at $x/c_r = 0.75$ and 2.75, tip vortex (TV) and junction vortex (JV).

to be zero on the edges of the measurement plane. The lift-induced drag D_i was then obtained by

$$D_i = \frac{1}{2}\rho_\infty \iint_{S\zeta} \psi\zeta \, \mathrm{d}y \, \mathrm{d}z - \frac{1}{2}\rho_\infty \iint_{S1} \phi\sigma \, \mathrm{d}y \, \mathrm{d}z \tag{3}$$

where ζ is the vorticity, the surface S_ζ is the region within $S1$ where the vorticity is nonzero, $\sigma(=\partial v/\partial y + \partial w/\partial z)$ is a source term, and the flow is incompressible. C_{Di} of 0.021 was observed for $x/c_r = 2.75$. C_{Di} values were also estimated from the following Prandtl's inviscid, incompressible lifting-line equation:

$$D_i = L \sin\alpha_i = L \sin\alpha_i(z_0) = \frac{1}{4\pi U_\infty} \int_{-b/2}^{b/2} \left[\frac{(\mathrm{d}\Gamma/\mathrm{d}z)\,\mathrm{d}z}{z - z_0} \right] \cdot L \tag{4}$$

where α_i is the induced angle of attack. Prandtl's classical lifting-line theory (for high Reynolds number or inviscid flow and high-aspect-ratio wings) was found to overpredict the lift-induced drag for a low-aspect-ratio wing at $Re = 1.81 \times 10^5$; an order of magnitude larger than those computed from Eq. (4) was observed.

Winglet Dihedral

The effects of winglet dihedral, $\delta = 0, \pm 20, \pm 40, \pm 67.5$, and ± 87.5 deg, on the nondimensional tip-vortex flow structure are presented in Fig. 5. The constant increment levels of $\zeta c_r/u_\infty$ and u/u_∞ are 1.5 and 0.025, respectively. For clarity, only the wake surveys in the wing tip/winglet region at selected δ and $x/c_r = 0.75$ and 2.75 are presented. The dashed lines denote the position of the trailing edge of the wing and winglet. The ***vw*** crossflow vectors (not shown in Fig. 5) indicate that the addition of a winglet, in general, displaced

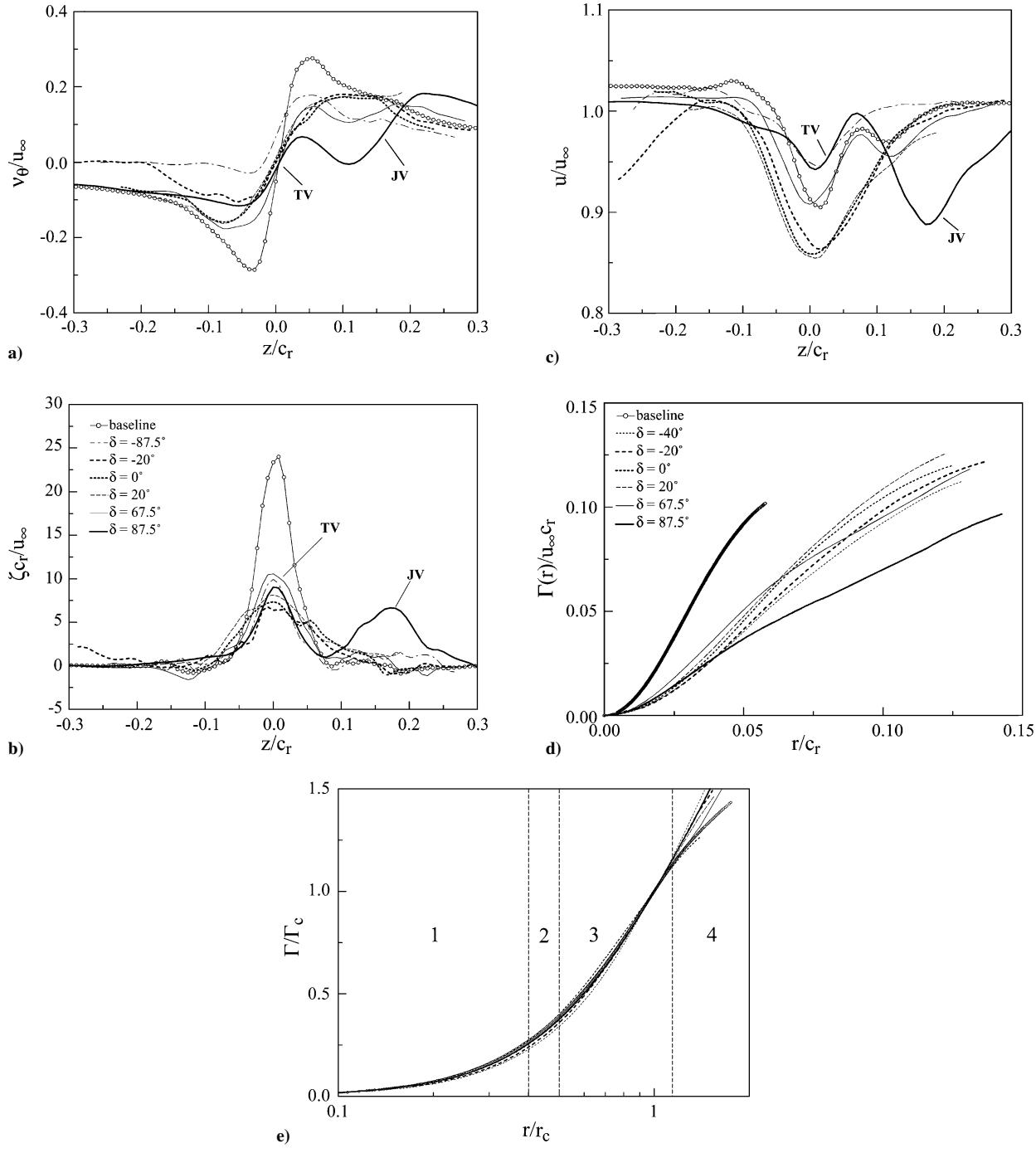

Fig. 6 Vortex flow quantities across the vortex center at $x/c_r = 2.75$. 1, inner region; 2, buffer region; 3, logarithmic region; and 4, outer region, tip vortex (TV) and junction vortex (JV).

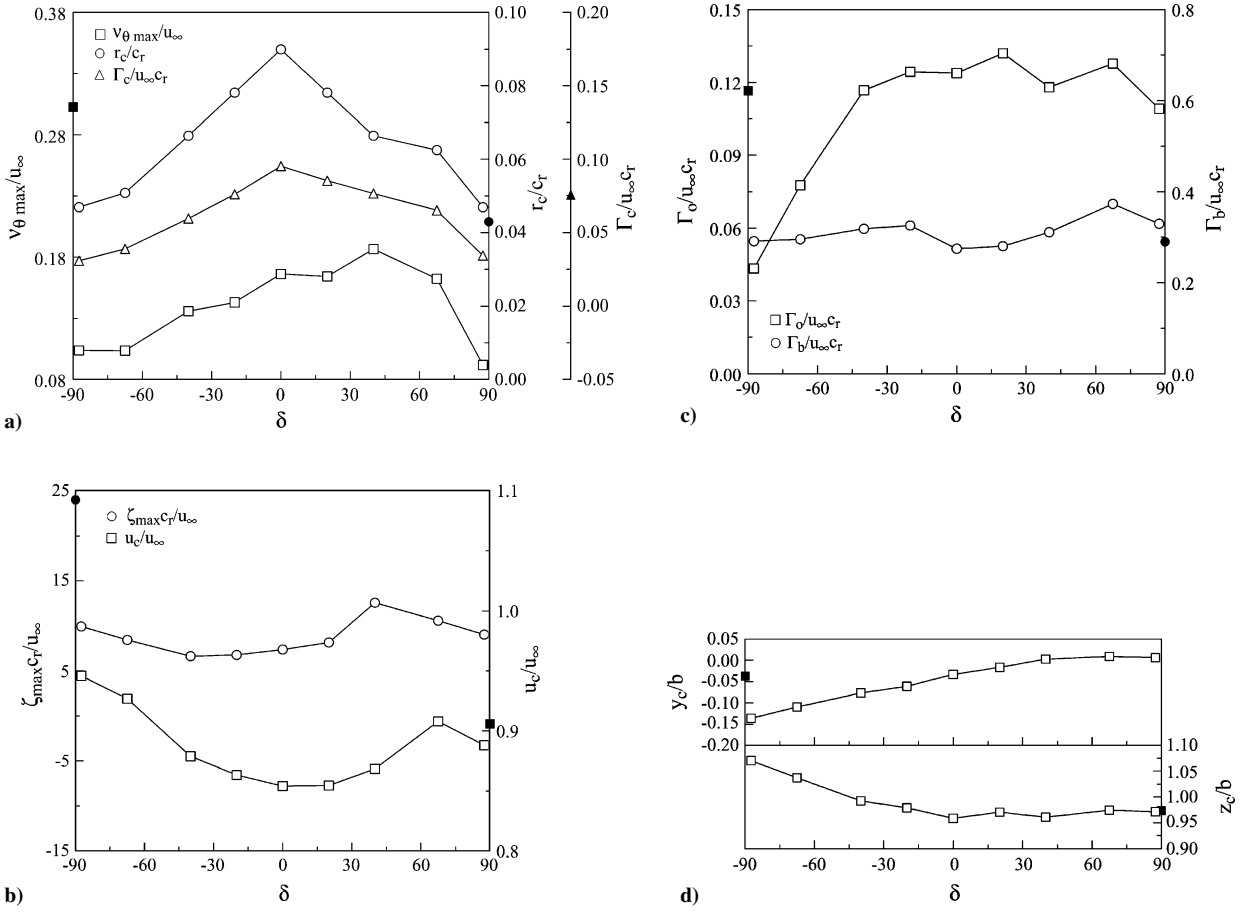

Fig. 7 Variation of critical vortex flow quantities with δ at $x/c_r = 2.75$: solid symbol, baseline wing.

or diffused the tip-vortex flow along the winglet span, reducing the inflow above the wing, and caused a small increase in the velocity behind the tip of the surface. Also, in addition to the tip vortex and wing wake observed behind a baseline wing (Figs. 2a and 2b), the addition of a winglet also produced a junction vortex, or a secondary vortical structure, immediately downstream of the winglet at $x/c_r = 0.75$, regardless of the magnitudes of the winglet dihedral tested. The junction vortex was generally smaller in size and with lower value of vorticity compared to the tip vortex. The strength and velocity deficit of the junction vortex increased with increasing positive δ while decreasing with x/c_r (Fig. 5). The junction vortex moved outboard and upward toward the tip vortex, with the tip vortex moving inboard and downward with increasing positive winglet dihedral as it moved downstream. The tip vortex and the junction vortex coalesced into a well-organized vortex (for $\delta = 0, \pm 20, \pm 40, -67.5$, and to some extent -87.5 deg) at $x/c_r = 2.75$ with the overall behavior of the vortex flow quantities resembling that of a baseline wing. For high positive winglet angle ($\delta = 67.5$ and, especially, 87.5 deg), the junction vortex remained prominent and paired with the tip vortex.

The nondimensional distributions of v_θ, ζ, and u_c through the tip vortex at selected δ and $x/c_r = 2.75$ are shown in Fig. 6. The existence of the junction vortex, or the vortex pair, for $\delta = 87.5$ deg and, to a lesser extent, for $\delta = 67.5$ deg is clearly seen. Also, as a result of the reduction of the total energy of the crossflow circulation, the tangential velocity and vorticity distributions (Figs. 6a and 6b) were of lower magnitudes and, consequently, with a higher value of core radius, compared to a baseline wing. Moreover, similar to a baseline wing, the axial velocity profiles persistently displayed a wakelike nature for all of the winglet dihedrals tested (Fig. 6c). The variation of the critical vortex flow quantities, including the circulation and the trajectory of the vortex, with δ at $x/c_r = 2.75$ is summarized in Fig. 7.

Figure 7a shows that the peak tangential velocity increased almost linearly with δ (for $-87.5 \le \delta \le 40$ deg), reaching a local maximum with $v_{\theta\text{peak}} = 0.187u_\infty$ (compared to $0.3u_\infty$ of a baseline wing) at $\delta = 40$ deg, and began to drop rapidly to $v_{\theta\text{peak}} = 0.09u_\infty$ at $\delta = 87.5$ deg. In the meantime, both the core radius and the core circulation were found to increase linearly with increasing δ, reaching a local maximum at $\delta = 0$ deg with $r_c = 0.09c_r$ and $\Gamma_c = 0.095u_\infty c_r$ (compared to $r_c = 0.043c_r$ and $\Gamma_c = 0.074u_\infty c_r$ of a baseline wing), and started to drop linearly to $r_c = 0.047c_r$ and $\Gamma_c = 0.034u_\infty c_r$ at $\delta = 87.5$ deg. No significant difference in the values of r_c and Γ_c was observed between $\delta = -87.5$ and 87.5 deg. The values of r_c ($v_{\theta\text{peak}}$ and ζ_{peak}) were always above (below), irrelevant to the magnitudes of δ, those of a baseline wing. Note that a reduction in $v_{\theta\text{peak}}$ or an increase in r_c has been used by some experimenters as a measure of reduced vortex hazard. The increased r_c of the tip vortex for any δ, compared to a baseline wing, also suggests that the vortex was more resistant toward the diffusion influence of turbulence. Figures 7a and 7b also show that the negative δ produced a slightly lower (higher) Γ_c and $v_{\theta\text{peak}}(u_c)$ than the positive δ and that the r_c values remained unchanged between the negative and positive dihedrals of same absolute magnitude.

Figure 7b also shows that for a wing/winglet configuration, the magnitude of u_c was always below the freestream value. The u_c was slightly above the baseline-wing value for $\delta = -87.5$ and -67.5 deg and was reduced to below the baseline-wing value with increasing δ. A local minimum of $u_c = 0.854u_\infty$, compared to $u_c = 0.905u_\infty$ of a baseline wing, was obtained at $\delta = 0$ deg. For $\delta > 0$ deg, the core axial velocity increased with δ up to $\delta = 67.5$ deg and was followed by a slight drop at $\delta = 87.5$ deg. Note that the observed decrease–increase trend in the variation of u_c with δ was found to be opposite to that of r_c and Γ_c for a wing/winglet configuration. Furthermore, whereas the addition of a winglet did not alter substantially the amount of bound circulation (due to the small variation in the effective wing span for

a same lift coefficient condition), as is shown in Fig. 7c, however, it varied the spanwise $\Gamma(z)$ distributions (Fig. 4), moving the center of vorticity further outboard along the span (Fig. 7d). On the other hand, the total circulation of the vortex was found to increase drastically with δ for $-87.5 \le \delta \le -40$ deg, and reached a rather constant value, comparable to that of a baseline wing, for $-40 \le \delta \le 87.5$ deg.

The behavior of the spanwise $\Gamma(z)$ and radial $\Gamma(r)$ distributions and the inner-flow self-similarity of the tip vortex at different δ for $x/c_r = 2.75$ are presented in Figs. 4, 6d, and 6e, respectively. Figure 4 indicates that the $\Gamma(z)$ distribution near the tip was more gradual with decreasing δ and shifted farther inboard (except for $\delta = 87.5$ deg, which exhibited the most precipitous dip near the tip), compared to a baseline wing. Also, the $\Gamma(r)$ level was found to significantly decrease below the baseline-wing value for a wing with a winglet (Fig. 6d). Note the significant reduction in the $\Gamma(r)$ distribution at $\delta = 87.5$ deg. Furthermore, when $\Gamma(r)/\Gamma_c$ is plotted against $\log(r/r_c)$, the inner region of the tip vortex in the near field behind a swept and tapered wing with and without a winglet also exhibits some interesting characteristics (Fig. 6e). The distribution of $\Gamma(r)$ within the tip vortex core followed an $\Gamma \propto r^2$ profile for $r/r_c < 0.4$ and varied logarithmically for $0.5 < r/r_c < 1.4$, a phenomenon similar to that of a square-tipped rectangular wing.[11,16] For $r/r_c > 1.4$, Γ continued to vary with x/c_r, suggesting that at $r > 1.4r_c$, the rollup of the inner region of the vortex was only nearly complete and that there was a slow addition of vorticity to the outer layers of the vortex from the shear layer arriving from the inboard regions. The empirical curve-fit relationships that describe the inner-core region and the region where the $\Gamma(r)$ distribution is logarithmic, according to Hoffmann and Joubert[17] and Phillips,[18] are

$$\Gamma(r)/\Gamma_c = A(r/r_c)^2 \quad \text{for} \quad r/r_c < 0.4 \tag{5}$$

$$\Gamma(r)/\Gamma_c = B\log(r/r_c) + C \quad \text{for} \quad 0.5 < r/r_c < 1.4 \tag{6}$$

The curve-fit constants obtained at different x/c_r with an autocorrelation coefficient of 0.9994 are listed in Table 3.

Table 3 Curve-fit constants of Eqs. (5) and (6) at $x/c_r = 2.75$

δ, deg	A	B	C	δ, deg	A	B	C
Baseline	1.724	2.059	0.985	−20	1.755	2.169	1.003
0	1.722	2.067	0.985	−40	2.126	1.756	0.989
20	1.682	2.218	1.000	−67.5	2.204	1.843	0.998
40	1.801	2.151	1.002	−87.5	1.593	2.336	1.005
67.5	1.730	2.195	1.003				
87.5	1.984	1.988	0.995				

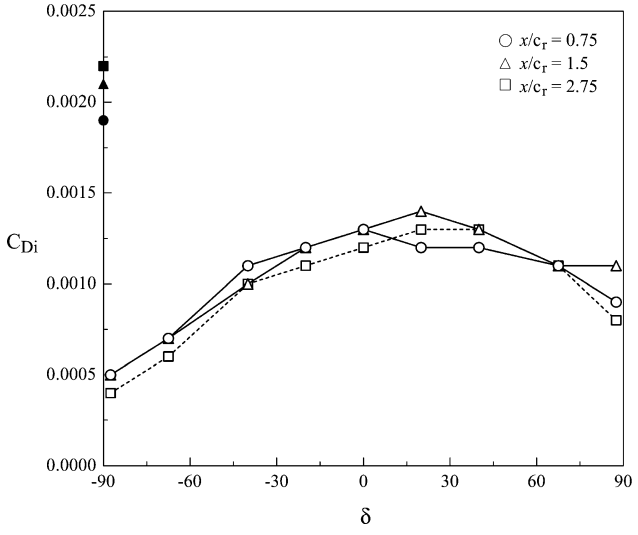

Fig. 8 Lift-induced drag coefficient.

Finally, the variation of C_{Di}, computed based on the Maskell method [Eq. (3)], with δ is summarized in Fig. 8. Compared to a baseline wing, a 38–81% reduction in C_{Di}, depending on the values of δ and, to a much lesser extent, the downstream distance, was observed. The $\delta = -87.5$ deg case provided the highest C_{Di} reduction. The averaged values (in the near field) of C_{Di} first increased with δ, reaching a local maximum at about $\delta = 20$ deg, and started to decrease slightly with increasing positive δ. The data also indicate that the negative winglet dihedral yielded a lower C_{Di} than the corresponding positive dihedral case (a result which agrees with the observation of Gold and Visser[7]). Also, the addition of a winglet, regardless of δ, increased the total drag (lift-induced drag and profile drag), compared to the baseline, as a result of the increase in the total wing surface area and the flow separation promoted by the nonoptimum wing tip and winglet junction (Fig. 3c). The 67.5-deg dihedral winglet, however, produced the least increase (decrease) in the total drag (L/D ratio) compared to a baseline wing (Figs. 3a and 3b). The values of C_{Di} at different δ were also estimated by using the classical lifting-line theory [Eq. (5)]. Similar to a baseline wing, the C_{Di} calculated by Eq. (5) was found to be an order of magnitude higher than those computed based on the Maskell method.

Conclusions

The three-dimensional tip-vortex flow behind a swept and tapered NACA 0015 wing with and without winglet was investigated at $C_L = 0.73$ and $Re = 1.81 \times 10^5$. For a baseline wing, the inner region of the tip vortex was nearly axisymmetric with $\Gamma_c/\Gamma_o = 0.63$ and $\Gamma_o/\Gamma_b = 0.4$ for $x/c_r = 2.75$. The inner flow of the tip vortex of a wing with and without winglet exhibited a self-similar behavior. The winglet dihedral led to a significantly reduced (increased) $v_{\theta\text{peak}}$ and $\zeta_{\text{peak}}(r_c)$ compared to a baseline wing. The value of $\Gamma_c(u_c)$, however, increased (decreased) above (below) the baseline-wing value with decreasing $|\delta|$, reaching a local maximum (minimum) at $\delta = 0$ deg, and started to drop (rise) with increasing $|\delta|$. C_{Di} was always reduced by the addition of a winglet. The negative winglet dihedral was more effective in reducing C_{Di} compared to the winglet of positive dihedral. A large discrepancy in the lift-induced drag was, however, observed between the wake integral method and the classical lifting-line theory. Also, note that the present investigation was undertaken with the goal of quantifying the effect of the dihedral of a simple swept and tapered winglet on the tip-vortex flow; the winglet of this investigation is undoubtedly not optimum.

Acknowledgments

This work was supported by the Natural Sciences and Engineering Research Council of Canada.

References

[1]Patterson, J. C., "Vortex Attenuation Obtained in the Langley Vortex Research Facility," *Journal of Aircraft*, Vol. 12, No. 5, 1975, pp. 745–749.

[2]Whitcomb, R. T., "A Design Approach and Selected Wind-Tunnel Results at High Subsonic Speeds for Wing-Tip Mounted Winglets," NASA TN D-8260, July 1976.

[3]Spillman, J. J., "The Use of Wing Tip Sails to Reduce Vortex Drag," *Aeronautical Journal*, Vol. 82, Sept. 1978, pp. 387–395.

[4]Vijgen, P. M. H. W., van Dam, C. P., and Holmes, B. J., "Sheared Wing-Tip Aerodynamics: Wind-Tunnel and Computational Investigation," *Journal of Aircraft*, Vol. 26, No. 3, 1989, pp. 207–213.

[5]Naik, D. A., and Ostowari, C., "Effects of Nonplanar Outboard Wing Forms on a Wing," *Journal of Aircraft*, Vol. 27, No. 2, 1990, pp. 117–122.

[6]Eppler, R., "Induced Drag and Winglets," *Aerospace Science and Technology*, Vol. 1, No. 1, 1997, pp. 3–15.

[7]Gold, N., and Visser, K. D., "Aerodynamic Effects of Local Dihedral on a Raked Wingtip," AIAA Paper 2002-0831, 2002.

[8]Smith, H. C., "Method for Reducing the Tangential Velocities in Aircraft Trailing Vortices," *Journal of Aircraft*, Vol. 17, No. 12, 1980, pp. 861–866.

[9]Gu, W., Robinson, O., and Rockwell, D., "Control of Vortices on a Delta Wing by Leading-Edge Injection," *AIAA Journal*, Vol. 31, No. 7, 1993, pp. 1177–1186.

[10]Wenger, C. W., and Devenport, W. J., "Seven-Hole Pressure Probe Calibration Utilizing Look-Up Error Tables," *AIAA Journal*, Vol. 37, No. 6, 1999, pp. 675–679.

[11]Birch, D., Lee, T., Mokhtarian, F., and Kafyeke, F., "Structure and Induced Drag of a Tip Vortex," *Journal of Aircraft*, Vol. 41, No. 5, 2004, pp. 1138–1145.

[12]Chow, J. S., Zilliac, G. G., and Bradshaw, P., "Mean and Turbulence Measurements in the Near Field of a Wingtip Vortex," *AIAA Journal*, Vol. 35, No. 10, 1997, pp. 1561–1567.

[13]Lamb, H., *Hydrodynamics*, 6th ed., Dover, New York, 1945, p. 592.

[14]Glauert, T. H., *The Elements of Airfoil and Airscrew Theory*, Cambridge Univ. Press, London, 1926.

[15]Maskell, E., "Progress Towards a Method for the Measurement of the Components of the Drag of a Wing of Finite Span," Royal Aircraft Establishment, RAE Technical Rept. 72232, 1973.

[16]Ramaprian, B. R., and Zheng, Y., "Measurements in Rollup Region of the Tip Vortex from a Rectangular Wing," *AIAA Journal*, Vol. 35, No. 12, 1997, pp. 1837–1843.

[17]Hoffmann, E. R., and Joubert, P. N., "Turbulent Line Vortices," *Journal of Fluid Mechanics*, Vol. 16, 1963, pp. 395–411.

[18]Phillips, W. R. C., "The Turbulent Trailing Vortex During Roll-Up," *Journal of Fluid Mechanics*, Vol. 105, 1981, pp. 451–467.